# Tiger-3D: 2D/1D Coupled Whole-core Transport Code Based on Large-Scale Parallel Computation

Wenbin Wu [a, b,*], Qing Li [a] and Kan Wang [b]

[a] *Science and Technology on Reactor System Design Technology Laboratory, Nuclear Power Institute of China, Chengdu, 610041, China.*
[b] *Department of Engineering Physics, Tsinghua University, Beijing, 100084, China*
[*]Corresponding author: wenbinwu@126.com

## 1. Introduction

With the fast advance of computing technology, a number of researchers [1-4] have recently developed 2-D/1-D coupled methods for 3-D neutron transport. Typical reactors are much heterogeneous in the radial direction while relatively homogenous in the axial direction. 2-D/1-D methods take advantage of this geometric feature, thus obtaining good accuracy and efficiency. In 2-D/1-D methods, 3-D problems are divided axially into homogenous 2-D planes, which are solved by 2-D method of characteristics. Then 2-D MOC is coupled with 1-D diffusion or transport solvers in the framework of 3-D coarse mesh finite difference (CMFD) formulation.

Generally, 2-D planes are solved independently, and this axial parallel degree is adopted in most 2-D/1-D methods. However, the number of 2-D planes is about 30 for typical reactors, which is too small to utilize large-scale clusters. Some codes like DeCART adopt parallel features of angles in 2-D MOC simultaneously. However, the number of cores being used is still much smaller compared with that modern supercomputers could provide. It's therefore desired to develop a 2-D/1-D method based on large-scale parallel computation. In this work, except for the axial parallel degree, spatial domain decomposition is radially adopted. Large-scale parallel computation is realized by combining parallel degrees of both directions of 2-D/1-D method. In this summary, we provide basic theory and preliminary numerical results.

## 2. Theory

### 2.1 2-D/1-D Scheme

Starting from the 3-D Boltzmann transport equation for a particular angle m and energy group g (Eq. 1):

$$\xi_m \frac{\partial \psi_g(\mathbf{r},\mathbf{\Omega}_m)}{\partial x} + \eta_m \frac{\partial \psi_g(\mathbf{r},\mathbf{\Omega}_m)}{\partial y} + \mu_m \frac{\partial \psi_g(\mathbf{r},\mathbf{\Omega}_m)}{\partial z} + \Sigma_{t,g}(\mathbf{r})\psi_g(\mathbf{r},\mathbf{\Omega}_m) = Q_g(\mathbf{r},\mathbf{\Omega}_m) \quad (1)$$

where the denotation is standard and the source Q is the sum of the fission and scattering sources.

Integrating over a 2-D plane axially [4] and moving the axial streaming to the right hand side, the 2-D equation for plane k is yielded as Eq. (2):

$$\xi_m \frac{\partial \psi_{g,m,k}(x,y)}{\partial x} + \eta_m \frac{\partial \psi_{g,m,k}(x,y)}{\partial y} + \Sigma_{t,g,k}(x,y)\psi_{g,m,k}(x,y)$$
$$= Q_{g,k}(x,y) - TL^{Axial}_{g,m,k}(x,y) \quad (2)$$

where the transverse leakage source $TL^{Axial}_{g,m,k}(x,y)$ is denoted by neutron currents at the top (T) and bottom (B) of each plane:

$$TL^{Axial}_{g,m,k}(x,y) = \frac{1}{4\pi\Delta z_k}\left[J_{g,k}(z^T) - J_{g,k}(z^B)\right] \quad (3)$$

Eq. (2) is a transport equation of 2-D heterogeneous planes, which are solved by 2-D MOC. Then, cells are homogenized by 2-D solutions.

Similarly, integrating radially over homogenized cell p, we obtain 1-D transport equation:

$$\mu_m \frac{d\psi^p_{g,m}(z,\mu_m,\varphi_m)}{dz} + \Sigma_{t,g,p}(z)\psi^p_{g,m}(z,\mu_m,\varphi_m) =$$
$$Q^p_g(z) - TL^{Radial}_{g,m,p}(z,\mu_m,\varphi_m) \quad (4)$$

Denoting $TL^{Radial}_{g,m,p}(z,\mu_m,\varphi_m)$ by currents, adopting diffusion approximation and solving Eq. (4) by finite difference method, Eq. (5) was yielded:

$$\frac{1}{\Delta z}\left(J^p_{g,z+} - J^p_{g,z-}\right) + \Sigma_{t,g,p}\phi_{g,p} = \frac{\chi_g}{k_{eff}}\sum_{g'=1}^{G}\left(\nu\Sigma_f\right)_{g',p}\phi^p_{g'} + \sum_{g'=1}^{G}\Sigma_{s0,g'-g,p}\phi^p_{g'}$$
$$-\left(\frac{1}{\Delta x}\left(J^p_{g,x+} - J^p_{g,x-}\right) + \frac{1}{\Delta y}\left(J^p_{g,y+} - J^p_{g,y-}\right)\right) \quad (5)$$

Solving Eq. (2) and Eq. (5) alternately [2-4] and transferring radial and axial leakage terms between them in the framework of 3-D CMFD formulation, results of Eq. (1) can be obtained.

### 2.2 2-D MOC Based on Spatial Domain Decomposition

In this work, Eq. (2) is solved by 2-D matrix MOC based on spatial domain decomposition. Matrix MOC was proposed by Zhang HB[5], in which a linear algebraic equation system (Eq. 6) represented by coefficient-matrix was formed by sweeping only once, and then solving the linear system took the place of repeatedly characteristics sweeping.

$$Ax = Bq \quad (6)$$

Furthermore, the coefficient-matrices A and B have good sparsity and numerical features, which reduce significantly the constructing computation and memory demand.

As to the spatial domain decomposition, multi-domain coupled PGMRES algorithm is proposed for directly

solving the domain-decomposed matrix MOC equations. In this algorithm, convergence of iterations of angular flux at inner boundaries is improved. PGMRES algorithm in matrix free mode is provided by PETSc library [6] maintained by ANL.

### 2.3 1-D Solver Embedded Into 3-D CMFD

Moving the radial leakage term to the left hand side, Eq. (5) turns out to be a 3-D CMFD equation, thus the 1-D axial diffusion solver is embedded or hidden into the 3-D CMFD formulation.

It should be noted that the 3-D CMFD equation is decomposed completely in both radial and axial directions, making it rough to handle. Similarly, PGMRES algorithm in matrix free mode from PETSc library is adopted, and the matrix-vector multiplication denoted by direct finite difference instead of explicit matrix is passed to the PGMRES solver interface.

### 2.4 Large-scale Parallel Computation Model

For this 2-D/1-D scheme, spatial domain decomposition is radially adopted by 2D matrix MOC, while planes are independent axially. Thus, large-scale parallel computation is realized by combining parallel degrees of both directions. According to the theory above, Tiger-3D code is developed.

In Tiger-3D code, each process deals with a sub-domain of 2-D plane. All the processes are mapped into three-dimensional topo-structure. Radial and axial MPI communicators are defined to manage the message passing.

For typical PWR, the height is about 3.5m, and there are about 157 assemblies. Dividing it into 30 planes, and each process dealing with 1/4 assembly, totally 18840 computing cores can be utilized.

## 3. NUMERICAL RESULTS

Two benchmarks are analyzed using the Tiger-3D code. The calculation parameter is: 6 polar angles (0, $\pi$ ), 32 azimuths (0, $2\pi$ ), ray spacing ~0.01 cm, ~30 meshes in each fuel cell. The computing platform is a cluster with Intel SandBridge E5-2670 CPU linked by Infinite band network.

### 3.1 5-Pin Benchmark

This problem contains five pins, among which the centered one is changeable. There are three cases according to the centered pin: (1) Single Pin (SP), (2) Inner Moderator (IM) and (3) Control Rodded (CR). Refer to reference [7] for detailed descriptions.
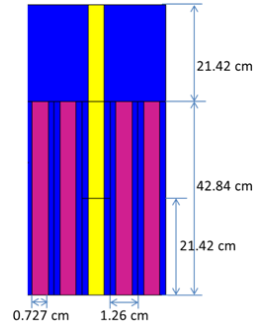


Fig. 1. Layout of 5-Pin benchmark problem

As shown in Tab. 1, the multiplication factor calculated by Tiger-3D is compared to the reference solution provided by Monte Carlo code RMC developed in Tsinghua University. For all three cases, Tiger-3D shows good agreement with the reference code, with maximum error -57 pcm.

Tab. 1. Numerical results of 5-Pin benchmark

| Case | SP | | IM | | CR | |
|---|---|---|---|---|---|---|
| | $k_{eff}$ | Err (pcm) | $k_{eff}$ | Err (pcm) | $k_{eff}$ | Err (pcm) |
| Ref. | 1.27088 | $\pm 11$ | 1.26772 | $\pm 11$ | 1.19451 | $\pm 12$ |
| Tiger-3D | 1.27031 | -57 | 1.26810 | 38 | 1.19428 | -23 |

### 3.2 3-D C5G7 Benchmark

3-D C5G7 benchmark [8, 9], posted by OECD/NEA, represents a small PWR core with 4 active fuel assemblies, and is widely calculated by many codes for verification. The problem specifications consist of the core geometry data and the seven group macroscopic cross sections specified for each material. There are four configurations defined as: Original, Unrodded, Rodded A, and Rodded B. In this work, Tiger-3D calculates the eighth symmetric reactor.

For the extended cases, they are axially divided into four planes, while each plane is separately divided into 7, 7, 7, and 10 sub-planes for 1-D solver. Radially two domain decomposition modes are used as shown in Tab. 2.

Tab.2. Domain decomposition modes for radial solver

| Domain Decomposition Modes | Total Processes (#) |
|---|---|
| $10 \times 10$ | 220 |
| $16 \times 16$ | 544 |

The numerical results for the extended cases are demonstrated in Tab. 3. The eigenvalue errors are separately -85 pcm, -55 pcm, -102 pcm for unrodded, rodded A, rodded B cases. For all three cases, the maximum axially integrated pin power error is 1.50%, and the maximum slice integrated pin power error is 4.0% located at slice #3.

For the original case, it is axially divided into 10 planes, while each plane is divided into 10 sub-planes. Each plane is assigned 10 processes, and totally 100 processes are used. The numerical results are listed below. Eigenvalue error is 38 pcm. Assembly power

errors are -0.062%, 0.018%, and 0.094% for $UO_2$-1, MOX and $UO_2$-2. Pin power errors for the pins with maximum and minimum power are -0.151% and 1.391%. The total computational time is 162.2 seconds. These results agree well with the MCNP reference.

The overall accuracy of Tiger-3D is encouraging compared with the original benchmark participants, while the computation time is significantly reduced due to the large-scale parallel computation.

Tab. 3 Numerical results of 3D C5G7 by Tiger-3D

| Benchmark mode | | Unrodded | | Rodded A | | Rodded B | |
|---|---|---|---|---|---|---|---|
| Decomposing mode | | 10[①] | 16[②] | 10 | 16 | 10 | 16 |
| Eigenvalue Error, pcm | | -85 | -83 | -55 | -53 | -102 | -102 |
| Slice 1 Pin Power Error (%) | Maximum | 2.28 | 2.34 | 2.07 | 2.05 | 1.93 | 2.01 |
| | Mean | 0.95 | 0.95 | 0.57 | 0.57 | 0.41 | 0.41 |
| | RMS | 1.02 | 1.03 | 0.69 | 0.70 | 0.59 | 0.59 |
| | MRE | 0.37 | 0.37 | 0.21 | 0.21 | 0.16 | 0.16 |
| Slice 1 Assembly Error (%) | $UO_2$-1 | 0.67 | 0.66 | 0.23 | 0.22 | 0.00 | -0.01 |
| | MOX | 0.93 | 0.94 | 0.59 | 0.59 | 0.31 | 0.32 |
| | $UO_2$-2 | 1.08 | 1.09 | 0.69 | 0.70 | 0.56 | 0.56 |
| Slice 2 Pin Power Error (%) | Maximum | 1.89 | 1.88 | 1.81 | 1.84 | 1.76 | 1.78 |
| | Mean | 0.43 | 0.44 | 0.40 | 0.40 | 0.45 | 0.45 |
| | RMS | 0.57 | 0.59 | 0.50 | 0.51 | 0.56 | 0.57 |
| | MRE | 0.11 | 0.11 | 0.13 | 0.13 | 0.13 | 0.13 |
| Slice 2 Assembly Error (%) | $UO_2$-1 | 0.17 | 0.16 | 0.38 | 0.37 | -0.11 | -0.11 |
| | MOX | 0.39 | 0.40 | 0.31 | 0.32 | 0.49 | 0.50 |
| | $UO_2$-2 | 0.52 | 0.53 | 0.34 | 0.35 | 0.43 | 0.43 |
| Slice 3 Pin Power Error (%) | Maximum | 3.98 | 3.97 | 3.80 | 3.78 | 2.76 | 2.74 |
| | Mean | 2.38 | 2.37 | 2.19 | 2.19 | 1.70 | 1.69 |
| | RMS | 2.44 | 2.44 | 2.24 | 2.24 | 1.77 | 1.76 |
| | MRE | 0.48 | 0.48 | 0.34 | 0.34 | 0.22 | 0.21 |
| Slice 3 Assembly Error (%) | $UO_2$-1 | -2.21 | -2.22 | -1.98 | -1.99 | -1.99 | -1.99 |
| | MOX | -2.66 | -2.65 | -2.36 | -2.35 | -1.78 | -1.77 |
| | $UO_2$-2 | -2.12 | -2.11 | -2.05 | -2.04 | -1.34 | -1.33 |
| Axially Integrated Pin Power Error (%) | Maximum | 1.50 | 1.59 | 1.13 | 1.15 | 1.37 | 1.40 |
| | Mean | 0.26 | 0.27 | 0.22 | 0.22 | 0.28 | 0.29 |
| | RMS | 0.37 | 0.39 | 0.30 | 0.31 | 0.39 | 0.40 |
| | MRE | 0.18 | 0.19 | 0.18 | 0.18 | 0.24 | 0.25 |
| Integrated Assembly Error (%) | $UO_2$-1 | -0.08 | -0.09 | 0.01 | 0.00 | -0.23 | -0.24 |
| | MOX | 0.01 | 0.02 | -0.03 | -0.02 | 0.11 | 0.12 |
| | $UO_2$-2 | 0.24 | 0.26 | 0.05 | 0.06 | 0.20 | 0.21 |
| Outer Iter (#) | | 10 | 11 | 10 | 12 | 10 | 12 |
| Mat. Constr. Time (s) | | 4.84 | 1.84 | 4.80 | 1.80 | 4.79 | 1.86 |
| Total Time (s) | | 10.21 | 5.77 | 10.44 | 5.60 | 10.73 | 5.94 |

① Domain decomposition modes $10 \times 10$

② Domain decomposition modes $16 \times 16$

*3.3 Preliminary scaling results*

Preliminary parallel scaling results consist of two parts: radial scaling result and axial scaling result. As shown in Fig. 2, each process is assigned the task of $2\times2$ $UO_2$ cells drawn from C5G7 benchmark.
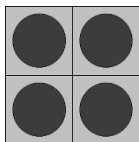
Fig. 2. Task of each process

For the radial scaling, the number of processes increases by square, i.e. $1^2, 2^2, 3^2... 20^2, 21^2$. Matrix construction time, linear solving time and total time are demonstrated in Fig. 3. As the number of processes increases, matrix construction time keeps nearly unchanged, while linear solving time increases very slowly.
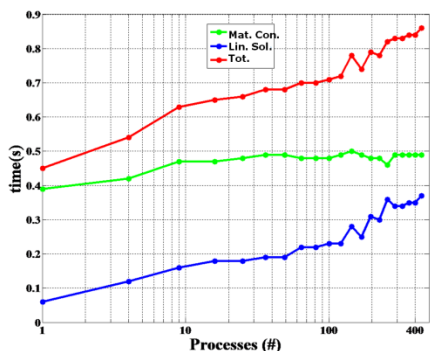
Fig. 3. Computational time for radial scaling result

For the axial scaling result, each plane is $16\times16$ $UO_2$ cells, accordingly $8\times8=64$ processes are used. As the number of planes increases, the total number of processes increases with 64 as the unit. Computational times are listed in Tab. 4. As the number of planes increases, the computational time increases slowly.

Tab. 4. Computational time for axial scaling result

| planes (#) | 1 | 2 | 3 | 4 | 5 |
|---|---|---|---|---|---|
| processes (#) | 64 | 128 | 192 | 256 | 320 |
| Mat. Con.(s) | 0.53 | 0.54 | 0.59 | 0.54 | 0.55 |
| Lin. Sol.(s) | 0.76 | 0.86 | 0.86 | 0.97 | 0.94 |
| Tot. (s) | 1.29 | 1.40 | 1.45 | 1.51 | 1.49 |
| planes (#) | 6 | 7 | 8 | 9 | |
| processes (#) | 384 | 448 | 512 | 576 | |
| Mat. Con.(s) | 0.54 | 0.55 | 0.54 | 0.57 | |
| Lin. Sol.(s) | 1.01 | 0.99 | 1.04 | 1.03 | |
| Tot. (s) | 1.55 | 1.54 | 1.58 | 1.60 | |

Good scalability is obtained in both radial and axial directions, and then we conclude that Tiger-3D should scale well for large-scale computation.

**4 Conclusions**

In this summary, a 2-D/1-D scheme based on large-scale parallel computation was proposed, and Tiger-3D code was developed. In Tiger-3D code, spatial domain decomposition was radially adopted, combined with natural parallel degree in the axial direction. The numerical results of two benchmarks demonstrated that the method could obtain good efficiency and accuracy. Future work will include testing Tiger-3D code on larger clusters, and further analyzing the scalability.

**References**

1   Xiao S. *Hardware accelerated high performance neutron transport computation based on AGENT methodology*, Ph.D. thesis, Purdue University, (2009).

2   Hursin M. *Full core, heterogeneous, time dependent neutron transport calculations with the 3D code DeCART*, Ph.D. thesis, University of California, Berkeley, (2010）.

3   Cho N Z, Lee G S. "Refinement of the 2-D/1-D fusion method for 3-D whole-core transport calculation," T*ransactions of the American Nuclear Society*, **87**, 417 (2003).

4   Takeda S K T. "Verification of 3D heterogeneous core transport calculation utilizing non-linear iteration technique," *Journal of Nuclear Science and Technology*, **41**(6), 645-654(2004).

5   Zhang H, Wu H, Cao L. "An acceleration technique for 2D MOC based on Krylov subspace and domain decomposition methods," *Annals of Nuclear Energy*, **38**, 2742-2751(2011).

6   Balay S, Brown J, Buschelman K, et al. "PETSc user's manual," Argonne National Laboratory, (2013).

7   Jin-Young Cho K K C L. "Axial SPn and radial MOC coupled whole core transport calculation," *Journal of Nuclear Science and Technology*, **44**(9), 1156-1171(2007)

8   M. A. SMITH and E. E. LEWIS, "Benchmark on deterministic transport calculations without spatial homogenization" NEA/NSC/DOC(2003)16, Nuclear Energy Agency Organization for Economic Co-Operation and Development(2003).

9   M. A. SMITH and E. E. LEWIS, "Benchmark on deterministic transport calculations without spatial homogenization: MOX fuel assembly 3-D extension case," NEA/NSC/DOC(2005)16, Nuclear Energy Agency Organization for Economic Co-Operation and Development(2005).